Geomorphology 488 (2025) 109954

Contents lists available at ScienceDirect

Geomorphology

journal homepage: www.journals.elsevier.com/geomorphology

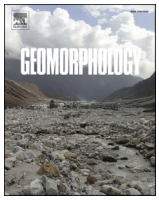

Neotectonics and paleoshoreline delineation of the Arabian Gulf using subsurface data and remote sensing techniques

Arsalan Ahmed Othman [a,*], Salahalddin S. Ali [b,c], Ahmed K. Obaid [d,e], Younus I. Al-Saady [f], Maher M. Mahdi [g], Mustafa Ali [f], Hasan Kattoof Jasim [d], Syed E. Hasan [h], Veraldo Liesenberg [i]

[a] Petroleum Engineering Department, College of Engineering, Komar University of Science and Technology, Sulaimaniyah 460013, Iraq
[b] Civil Engineering Department, College of Engineering, Komar University of Science and Technology, Sulaimaniyah 46013, Iraq
[c] College of Science, University of Sulaimani, Sulaymaniyah, Iraq
[d] Department of Geology, University of Baghdad, Al-Jadiryah Street, Baghdad, Iraq
[e] Department of Earth Sciences, University of Durham, Durham DH1 3LE, UK
[f] Iraq Geological Survey, Al-Andalus Square, Baghdad 10068, Iraq
[g] Department of Geology, College of Science, University of Basrah, Basrah, Iraq
[h] Department of Earth & Environmental Sciences, University of Missouri, Kansas City, MO 64110-2499, USA
[i] Department of Forest Engineering, Santa Catarina State University (UDESC), Lages, SC 88520-000, Brazil

ARTICLE INFO

Keywords:
Paleoshoreline
Arabian Gulf
Sumer
Ur
Uruk
Larsa
TPI
Hammar Formation
Neotectonics

ABSTRACT

About 5500 ± 500 years ago, the paleoshoreline of the Arabian Gulf rose 3.75 m above its present level and covered the Lower Mesopotamia Plain, resulting in the deposition of the Hammar Formation. Along and near the Gulf shoreline, several ancient human settlements, such as Ur and Uruk, were built. Nowadays, there is no clear indication of the spatial extent of the paleoshoreline, and no ground surveys or fieldwork to verify its exact location have been conducted. The present research aimed to fill this gap by delineating (1) the paleoshoreline of the Gulf, (2) neotectonics activities, and (3) the archaeological sites using remote sensing data, which were validated by fieldwork and available subsurface information. Our study has determined the spatial distribution of the paleoshoreline, which we conclude was located about 190 to 230 km northwest of the present-day shoreline. Folding in the Hammar Formation confirms that the study area underwent neotectonic uplift, especially in the eastern parts. We estimate the uplift rate to range between 0.3 mm·yr^{-1} and 1.5 mm·yr^{-1}. Using the Topographic Position Index, we have determined the location of almost all major archaeological sites that were located ~5 m higher than the surrounding area. Further studies are recommended to accurately determine the uplift rate using advanced techniques.

1. Introduction

The interactions between tectonics, climate, and lithology have a major influence on how landscapes evolve (Reyss et al., 1999; Keller and Pinter, 2002; Othman and Gloaguen, 2014). Landscape mapping is a fundamental tool for analyzing and visualizing geologic features and reconstructing a region's tectonics and landscape evolution (Karymbalis et al., 2013; Iacobucci et al., 2023). However, due to the thick Quaternary sedimentary cover (Fouad and Sissakian, 2011), the tectonic features in the Mesopotamia Plain, specifically in its southern part, are not discernible.

Iraq, situated in the Lower Mesopotamian Plain (LMP), is considered the oldest civilization in the world (Al-Ameri and Briant, 2019), and, as such, has been a focus of considerable archaeological and historical geographic studies. However, there is a dearth of research on the Quaternary stratigraphy, neotectonics activities, and sea level fluctuations in the region (Heyvaert and Baeteman, 2007; Hritz et al., 2012; Al-Ameri and Briant, 2019). Coastal areas, rivers, floodplains, and deltas, being the most suitable locations for ancient human settlements (Cooke, 1987), are directly impacted by sea level fluctuations, which, in turn, influenced settlement patterns and distribution of ancient human communities. Shorelines of the Gulf are a classic example of this nature-

* Corresponding author.
E-mail addresses: arsalan.aljaf@komar.edu.iq, arsalan.aljaf@geosurviraqi.industry.gov.iq (A.A. Othman), salah.saeed@komar.edu.iq (S.S. Ali), ahmed.k.obaid@durham.ac.uk (A.K. Obaid), maher.mahdi@uobasrah.edu.iq (M.M. Mahdi), Hasan.jasim@sc.uobaghdad.edu.iq (H.K. Jasim), hasans@umkc.edu (S.E. Hasan), veraldo.liesenberg@udesc.br (V. Liesenberg).

https://doi.org/10.1016/j.geomorph.2025.109954
Received 29 April 2025; Received in revised form 1 August 2025; Accepted 1 August 2025
Available online 6 August 2025

human nexus.

The Arabian (Persian) Gulf (referred to as the Gulf in this paper) is a NW-trending shallow epicontinental sea resulting from the collision between the Arabian and the Iranian plates during the Late Cretaceous and Mio-Pliocene period (Othman and Gloaguen, 2013a; Parker et al., 2020). The present Gulf represents the remnant of the Neo-Tethyan Ocean (Alavi, 1994) when the Gulf level was in the vicinity of the Strait of Hormuz ~14,000 yr BP, at an elevation of ~120 m below the present sea level (Lambeck, 1996). Thereafter, the LMP underwent marine transgression in the Middle Holocene (Late Northgrippian; Heyvaert and Baeteman, 2007). The Gulf coast moved a considerable distance inland to be close to the Sumerian civilization communities, such as Ur and Eridu, as revealed in the Sumerian cuneiforms (Jacobsen, 1960).

The timing and/or the elevation of the maximum Gulf transgression have been widely debated. Most researchers suggested that the maximum transgression of the Gulf occurred between 5000 and 6000 yr BP (Cooke, 1987; Lambeck, 1996; Teller et al., 2000; Aqrawi, 2001; Pournelle, 2003; Kennett and Kennett, 2006; Jotheri et al., 2018; Parker et al., 2020; Forti et al., 2022; Iacobucci et al., 2023). Deposition of the marine Hammar Formation, which presently underlies the fluvial sediments (Hudson et al., 1957), resulted from this transgression. Estimates of the maximum transgression level of the Gulf ranged between 2 and 3 m asl (Lambeck, 1996; Teller et al., 2000; Parker et al., 2020), mentioned a maximum rise of the transgression at 3.75 m, and Pournelle (2003) reported that the maximum transgression was ~4.5 m asl. Differing from all the above-mentioned studies, Iacobucci et al. (2023) proposed that the Gulf level was 3-6 m lower than the current sea level.

The above-mentioned differences in the Gulf coastline level resulted in variations in the shoreline location. However, all researchers agreed that the Gulf shoreline was far north of its present position (Larsen, 1975; Heyvaert and Baeteman, 2007; Iacobucci et al., 2023). Beke (1835) pointed out that the lateral ancient Gulf extended 750 km northwest of the present Gulf. Cooke (1987) suggested that the sea reached 400 km inland. Sarnthein (1972), Macfadyen and Vita-Finzi (1978), Aqrawi (1995), Aqrawi (2001), Kennett and Kennett (2006), and Milli and Forti (2019) suggested that the shoreline position was between ~270 and 260 km north of the present shoreline. Based on the above-mentioned statements, the minimum extent of the Gulf shoreline transgression is 260 km north of the present shoreline. This, in turn, would lead to the fact that the archaeological sites, such as Uruk, Larsa, Tall Al-Laham, Tall Um-Al-Aqareb, Girsu, and Ur, would be underwater, which is not the case. The present study aimed to decipher the exact location of the shoreline by integrating subsurface remote sensing, and GIS. Recently, there has been an increased interest in applying remote sensing, either stand-alone or in combination with deep learning algorithms, for archaeological studies (Kadhim and Abed, 2023): one of the objectives being archaeological site detection (Agapiou and Lysandrou, 2020; Thompson, 2020; Ben-Romdhane et al., 2023; Łabuz et al., 2023). While remote sensing data and techniques have been effectively used in morphotectonic studies (Obaid and Allen, 2017, 2019; Othman et al., 2019; Salar et al., 2022), it has rarely been employed to delineate shorelines, such as the Gulf shoreline (Iacobucci et al., 2023).

The three-fold objectives of the current study include: (1) determination of the paleoshoreline of the Gulf, (2) neotectonics activities, and (3) mapping the archaeological sites using remote sensing data and techniques. Delineation of the paleoshoreline of the Gulf and the prevailing environment in a period critical for one of the best-known ancient human civilizations, should provide a sound basis for future archaeological and paleoclimatic studies. Our research used archival information, geological field data, modern laboratory techniques, and remote sensing to accomplish our objectives. The outcome of this research should help resolve the debate on the past extent of the Arabian Gulf shoreline and provide realistic data for future reference and use.

2. Hammar Formation

The Gulf shoreline transgression resulted in the deposition of the marine Hammar Formation that was identified at various localities within the LMP (Milli and Forti, 2019). Hudson et al. (1957) studied the fauna of the Hammar Formation in samples collected from the Zubair No. 31 test-boring and the Nahr Umar wells near Basrah. They found the formation to consist of alluvial sediments occurring 6.4 m below the ground level. The formation is of the Middle Holocene age with a thickness of 6.1 m. The lower part of the formation (4.25 m) consists of coarse and very coarse unsorted sand, rarely cemented, and some silt. The sediments include small marine *gastropods* and *lamellibranchs*, which normally live in relatively quiet, clear water. The upper part of the formation (1.85 m) consists of gray clay with thin washes of shells, specifically *Abracadabra*, with *occasional crab debris* and an abundance of *echinoid debris* (Hudson et al., 1957). Macfadyen and Vita-Finzi (1978) found molluscan fauna within two sets of samples collected from a bridge over the Musharah River, similar to what was found by Hudson et al. (1957) and Macfadyen and Vita-Finzi (1978).

Yacoub et al. (1985) conducted an extensive drilling program comprising eight deep boreholes (~150 m in depth) and 127 shallow boreholes (~20 m deep) in the southern part of Mesopotamia as part of a project funded by the Iraq Geological Survey (GEOSURV). Yacoub et al. (1985) and several other researchers have studied the borehole cores. Based on paleontological evidence, they concluded that the marine transgression of the Gulf occurred at 5500 ± 500 yr BP and extended as far as Amara City in the east and to Nasiriya City in the west of Mesopotamia (Yacoub et al., 1985).

Salman (1993, 1997) studied 30 samples from 14 shallow boreholes and 20 samples from four deep boreholes to re-evaluate the paleoecology of the Hammar Formation. She emphasized marine transgression and the presence of the Hammar Formation at several locations. Al-Jumaily (1994) studied the distribution of Ostracoda in the southern part of Iraq. He studied 962 core samples (478 core samples containing Ostracoda) collected from 51 boreholes drilled by GEOSURV (Yacoub et al., 1985). Aqrawi (1995) performed radiocarbon dating on five boreholes (drilled by GEOSURV) and four near-surface samples. He documented the distribution of the Hammar Formation in the southern part of Mesopotamia (Aqrawi, 1995). From the above studies and our current investigations, we believe that the Hammar Formation is a key feature in determining the paleoshoreline of the Gulf, because it was deposited during the same period as the Sumerian.

2.1. Study area

The study area is part of the Mesopotamia Foredeep (MF) of the Zagros Mountains Belt (ZMB). The MF is a continental basin that lies between the Zagros deformational front from the northeast and the stable interior of the Arabian Platform from the southwest (Fouad and Sissakian, 2011). The deformation of the Mesopotamia Foredeep resulted from the ongoing collisional process between Arabia and Eurasia after the closure of the Neo-Tethys Ocean (Alavi, 2007; Alavi, 1994). The ZMB is considered one of the most active mountain regions in the world (McQuarrie, 2004). The Mesopotamian Basin is tectonically less active, which has subtle deformation compared with the other tectonic units of the ZMB (Berberian, 1995).

Mesopotamia is a vast lowland in southern Iraq, encompassing the lower parts of the Tigris and Euphrates river basins. It extends ~625 km northwest-southeast, from Samarra to Faw, with an average width of 225 km and an elevation of less than 55 m asl (Fig. 1). We selected the southern part of Mesopotamia as our study area (Fig. 1; area A) due to its proximity to the Gulf Coast and the presence of major historical centers and civilizations in this region. This area spans ~250,000 km^2 and features a flat plain with a maximum slope of 1.13°. It is primarily composed of Quaternary sediments (Yacoub, 2011a, 2011b).

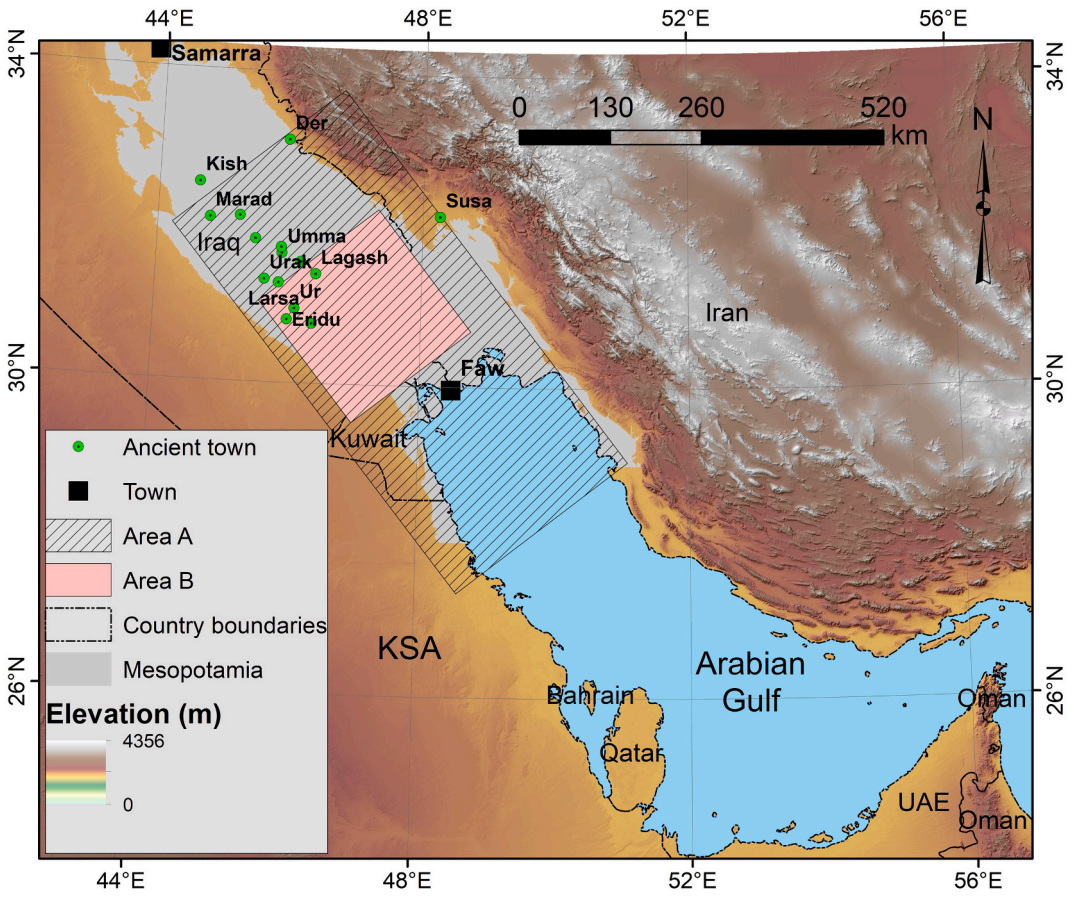

Fig. 1. Regional and location map of the study area.

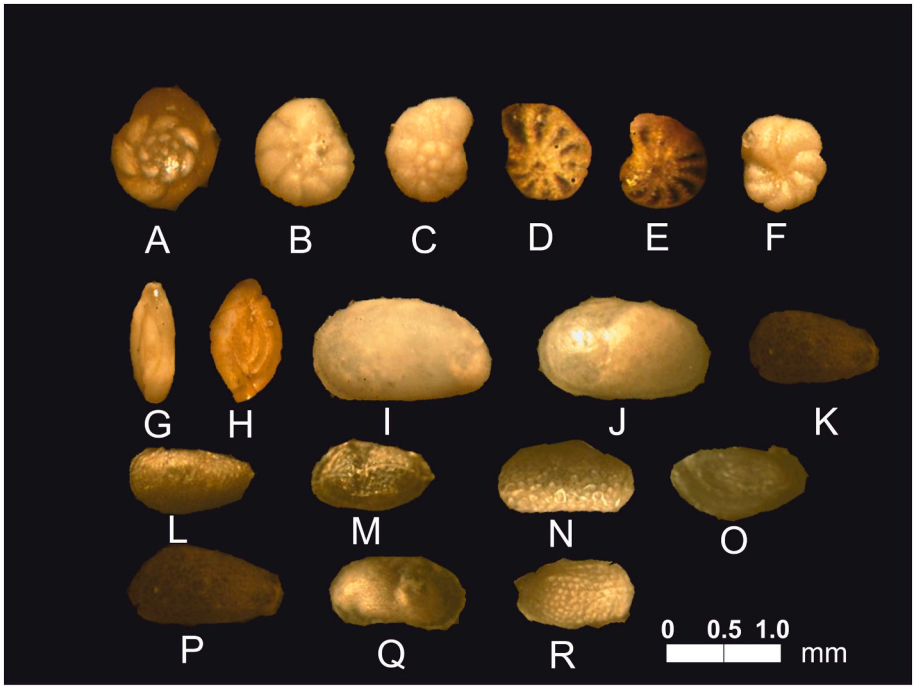

Fig. 2. Photos of identified fauna, Foraminifera species: A. Ammonia beccarii, B. Ammonia Parkinsoniana, C. Ammonia tepida, D. Elphidium advenum, E. Elphidium lessonii, F. Elphidum incertum, G. Quinqueloculina poeyana, H. Spiroloculina Laevigata. Ostracoda species: I. *Cyprideis torosa, J. Haplocytheria keyseri, K. Hemicytheridea paki, L. Carinocythereis indica, M. Neomonoceratina iniqua, N. Mediocytherideis (Sylvestra) seminist, O. Neocytheromorpha reticulata, P. Alocopocythere reticulate, Q. Neomonoceratina delicate, R. Loxoconcha* sp. (From a sample stored at the National Construction Center of Basrah, drilled in Khor Al-Zubair in 2007).

2.2. Hammar Formation fauna

Several groups of organisms have been recorded in the Hammar Formation samples. The important Foraminifera species identified by Al-Jaberi and Mahdi (2020) are listed in Appendix 1. While the Ostracoda species are reported by Al-Jumaily (1994), as shown in Appendix 1 and Fig. 2.

3. Materials and methods

3.1. Material

To accomplish this study, we used the data that came from the following sources which are satellite imagery, previous works, and fieldwork. We utilized Various types and scales of satellite imagery, including Landsat OLI, QuickBird, and the Digital Elevation Model (DEM) from the Shuttle Radar Topography Mission (SRTM V3).

Two free-of-cloud cover scenes of Landsat OLI images acquired on August 2, 2024, have also been used (Table 1). The Landsat OLI data have been atmospherically corrected employing the Fast Line-of-Sight Atmospheric Analysis of Spectral Hypercubes (FLAASH) algorithm to retrieve the at-surface reflectance (Felde et al., 2003).

Sixty-three QuickBird scenes with 60 cm spatial resolution, acquired in May 2006, have been used to verify the results and minimize fieldwork efforts. Moreover, 53 scenes of DEM with 30 m spatial resolution have been used to extract the topography of the Mesopotamian plain and simulate the shape of the ancient Gulf model based on its previous sea level.

Landsat OLI data were processed using the Environment for Visualizing Images (ENVI) version 5.6 software (Exelis Visual Information Solutions, 2015). ArcGIS 10.8.1 was used to create the datasets and prepare the final maps (ESRI, 2021). We also utilized RockWorks, a comprehensive software for creating 2D and 3D maps, which are widely used to generate geological cross-sections (RockWare, 2024).

3.2. Methodology

3.2.1. Database building

To create the required database for the Hammar Formation within the Geographic Information System (GIS) environment, available maps (geological and archaeological) have been scanned at a resolution of 300 dpi. These maps have been registered with the UTM projection-zone 38 N. The database includes the location (x and y coordinates), upper contact, lower contact, depth, and thickness of the Hammar Formation, along with sources of this information. The collected information is drawn from Hudson et al. (1957), Macfadyen and Vita-Finzi (1978), Raji (1983), Yacoub et al. (1985), Yacoub (1992), Salman (1993), Aqrawi (1993), Al-Jumaily (1994), Karim et al. (1994), Aqrawi (1995), and Yacoub (2011a). This database has been used to create a vector shapefile (points). These points were interpolated employing an Inverse Distance Weighting (IDW) method to produce several rasters with a spatial resolution of 30 m. The outcome of the rasters' production was depth, thickness, and the spatial distribution of the Hammar Formation.

The database of the archaeological sites (Directorate of Antiquities, 1976) has been mapped as a point using ArcGIS 10.8.1 software, where each point represents a town or city. The importance of recognizing the ancient cities and towns is that these sites are located in the land (nonmarine) areas, i.e., beyond the reach of the present Gulf shoreline.

3.2.2. Fieldwork and sampling

To validate and overcome any deficiencies in previous sources of information, 27 specialized samples during five days of intensive fieldwork were collected to determine the distribution of the Hammar Formation. Some of these samples were collected using an excavator machine. These samples have been complemented by additional samples of the Hammar Formation obtained from the National Construction Center of Basrah, which was obtained from Khor Al-Zubair in 2007 using a drilling truck.

Paleontological data were culled from a robust body of literature, including foundational references such as Murray (1969), Al-Jumaily (1994), Rohling and Cooke (2003), Shareef and Mahdi (2015), and Al-Jaberi and Mahdi (2020). We meticulously reviewed and documented the majority of the microfossils that were identified in previous research. This comprehensive approach allowed us to enrich our analysis and provide a robust underpinning for our findings.

Fifty grams of loose sediment were utilized for faunal extraction. The friable samples underwent thorough washing with tap water and were subsequently passed through a 63 μm sieve before being dried in an oven, as outlined by Green (2013). In contrast, the compacted samples were processed using chemical methods to ensure effective extraction of the fauna, following the methodology proposed by Al-Shawi et al. (2019). The organisms in all samples were inspected and identified using a binocular microscope.

3.2.3. DEM simulation

Fifty-three scenes of DEM were mosaicked and thresholded with an elevation of 55 m to delineate the Mesopotamian Plain. The mosaicked DEM data were used to determine the Best Elevation Corresponding to the Paleoshoreline (BECP) empirically by comparing the trails with the spatial distribution of the Hammar Formation derived from the database (see Section 3.2.1. Database Building). Since the DEM does not have a decimal but rather an integer format, the BECP is not precisely defined, appearing to be between 3 m and 4 m. To find the exact BECP, the pixels of the elevations 3 m and 4 m were vectorized and interpolated using IDW with a depth space of 10 cm. The elevation of 3.7 m shows the BECP. Thereafter, to obtain a more homogeneous water body, we implemented a fill sink algorithm in the BECP raster to remove minor imperfections.

Based on fieldwork observations, the major archaeological sites are located at a higher elevation than the surrounding area. Therefore, the Topographic Position Index (TPI) algorithm, as described in Eq. (1) (Weiss, 2001; Othman and Gloaguen, 2017; Othman et al., 2018), was used to delineate the archaeological sites. To compute the TPI, we first calculated the average elevation of all pixels within a defined kernel. Then, we subtracted the elevation value of each pixel (DEM value) from this local average to obtain the TPI across the entire area.

$$TPI = E_c - \left(\frac{1}{nM}\sum_{i \in m} E_i\right) \quad (1)$$

Table 1
Characteristics of Landsat OLI (Pour et al., 2023).[a]

Bands	Spectral range /band center (nm)	Resolution (m)	Bands	Spectral range /band center (nm)	Resolution (m)
Band 1 Coastal	435–451/443	30	Band 6 SWIR1	1566–1651/1608.5	30
Band 2 Blue	452–512/ 482	30	Band 7 SWIR2	2107–2294/2155.5	30
Band 3 Green	533–590/ 561.5	30	Band 8 Pan	503–676/589.5	15
Band 4 Red	636–673/654.5	30	Band 10 TIRS1	10,600–11,190/10895	100
Band 5 NIR	851–879/865	30	Band 11 TIRS2	11,500–12,510/12005	100
Band 9 Cirrus	1363–1384/1373.5	30	/	/	/

[a] NIR is Near-Infrared, SWIR is Short-wave infrared, and TIRS is Thermal Infra-Red Sensor.

Negative TPI values indicate that the central pixel is situated lower than its average surroundings, while positive TPI values indicate that the central pixel is situated higher than the average. We used several kernels to select the optimum kernel size. 11, 21, 31, 51, 101, and 201 kernels have been tested. As a final step, we used omission accuracy to double-check the results using data generated from our fieldwork, QuickBird images, and previous data.

3.2.4. Present shoreline

The Modified Normalized Difference Water Index (MNDWI; Xu, 2006) was applied (Eq. (2)) to the surface reflectance bands of the Landsat OLI data to extract the present shoreline of the Gulf. The MNDWI concept is based on the difference in reflectance between the green and shortwave infrared (SWIR) bands between water and land (Othman et al., 2024, 2025). The benefit of this index is to depict the maximum reflectance of water in the green band, as the minimum reflectance of water is in the SWIR band. The MNDWI ranges between −1 and 1. The values ≥0.09 are water, and < 0.09 are land (Xu, 2006).

$$MNDWI = \frac{\rho 560\ nm - \rho 1610\ nm}{\rho 560\ nm + \rho 1610\ nm} \quad (2)$$

3.2.5. Determination of uplift rates

According to the principle of original horizontality, which declares that sedimentary rock layers are initially deposited in a horizontal or near-horizontal orientation due to gravity (Levin and King Jr, 2016). The Hammar Formation is affected by tectonic deformation after its

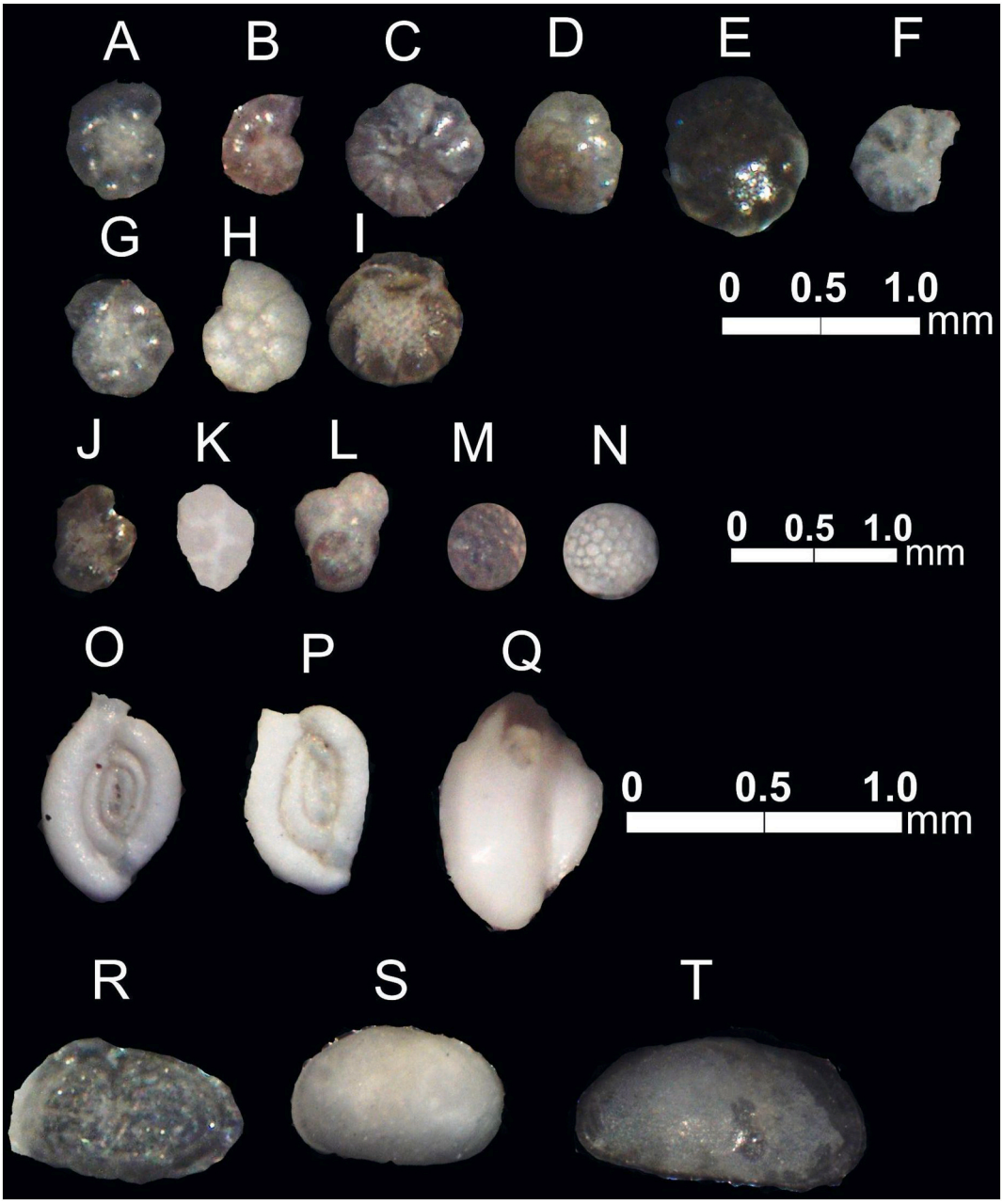

Fig. 3. Important marine fauna recorded in the Hammar Formation: A and G. *Haynesina* sp., B. *Elphidium excavatum*, C and I. *Ammonia beccari*, D. *Buccella frigida*, E. *Rosalina williansoni,* F. *Elphidium advenum*, H. *Ammonia tepida*., J, K, and L. planktonic foraminifera that transferred from deep to shallow water, M and N Radiolarian species, O. *Spiroloculina Laevigata,* P. *Spiroloculina eximia*, Q. *Triloculina oblonga,* R. *Alocopocythere reticulata*, S. *Cyprideis torosa,* T. *Haplocytheridea keyseri.* Where A-F, G-I, and T were collected from depth 4 m at site #HA8; D, E, J-Q, and S were collected from depth 5 m at site #HA7, and R was collected from depth 5 m at site #HA9. Note that the scale bar of A-I is 0.5 mm, that of J-N is 0.5 mm, and R-T is 0.5 mm.

horizontal deposition. To calculate the yearly rate of uplift within the Hammar Formation, we used a traditional method by measuring the difference between the highest and lowest points of the upper contact of each anticline in millimeters (Eq. (3)). Thereafter, we determine the highest and lowest points of the Halfayah, Majnoon, and Nahr Umar anticlines separately.

$$Uplift\ rate = \frac{Higest\ elevation\ (mm) - Lowest\ elevation(mm)}{Age\ of\ the\ deformed\ formation\ (year)} \quad (3)$$

4. Results

4.1. Hammar Formation samples: fauna

The foraminifera species that were recorded in the current study are shown in Figs. 2A-2D, 2F-2H, 2O, 3A, 3B, 3D, 3E, 3G, 3H, 3J-L, 3Q, and 3R. Several marine molluscan shells and bryozoa, characteristic of the Hammar Formation, were documented in this study and are illustrated in Fig. 4; the Ostracods species shown in Figs. 2I-Q and 3S (Appendix 1).

4.2. Ancient human settlements and present shoreline determination

The TPI results show that the best kernel to detect major archaeological sites is 201 by 201 pixels. This kernel enabled the detection of almost all of the major ancient settlements, including Uruk, Larsa, Ur, Tal Chukh, Girsu, and Tal Um-Al-aqareb. These sites were located at elevations exceeding 5 m above the surrounding area (Fig. 5).

Aqrawi (1995, 2001), Kennett and Kennett (2006), and Milli and Forti (2019) delineated the paleoshoreline of the Gulf with buffers of 260 km and 270 km at 5500 ± 500 yr BP. This statement is erroneous as it would imply that the ancient settlements were below the paleoshoreline (underwater) during 5500 ± 500 yr BP, which is not the houses (Fig. 6D).

4.3. Sea level change

The light blue polygon in Fig. 7 shows the paleoshoreline extracted from the SRTM DEM, and the dark blue polygon depicts the paleoshoreline of the Gulf delineated from field studies and sample analyses. The figure includes the location of the sites sampled by Hudson et al. (1957), Macfadyen and Vita-Finzi (1978), Raji (1983), Yacoub et al. (1985), Yacoub (1992), Aqrawi (1993), Salman (1993), Al-Jumaily (1994), Karim et al. (1994), Aqrawi (1995), and Yacoub (2011a) in addition to those sampled in this study. The red and green dots indicate the presence and absence of the Hammar Formation, respectively.

Fig. 8 shows the depth of the Hammar Formation. Yacoub et al. (1985), Al-Jumaily (1994), and Salman (1997) reported the maximum depth of the Hammar Formation at 14 m below the surface, at site #H4. This site is located 5 km east of Al-Zair village within the Missan Governorate. The minimum depth of the Hammar Formation is 0.5 m below the surface, found at site #H38, located 8.5 km northeast of Al-Tannuma town within the Basrah Governorate. The average depth of the Hammar Formation was ~6 m from the surface (Fig. 8).

Fig. 9 shows the distribution of the thickness and depth from the surface to the top of the Hammar Formation interpolated by employing IDW. The average thickness of the Hammar Formation is ~8.4 m; the maximum thickness is 21 m, found at site #H4 (Yacoub et al., 1985; Al-Jumaily, 1994; Salman, 1997); and the minimum thickness is 0.0 m, represented by the paleoshoreline of the Gulf at 5500 ± 500 yr BP.

5. Discussion

5.1. Paleoenvironment of the Gulf

We focused on two key groups of microorganisms (Foraminifera and Ostracoda) extracted from our field samples collected from the Hammar Formation. Many of these organisms thrive in mixed and variable environments characterized by fluctuating salinity levels, often inhabiting both estuarine and marine ecosystems. Consequently, this study paid particular attention to specific organisms that are exclusively found in

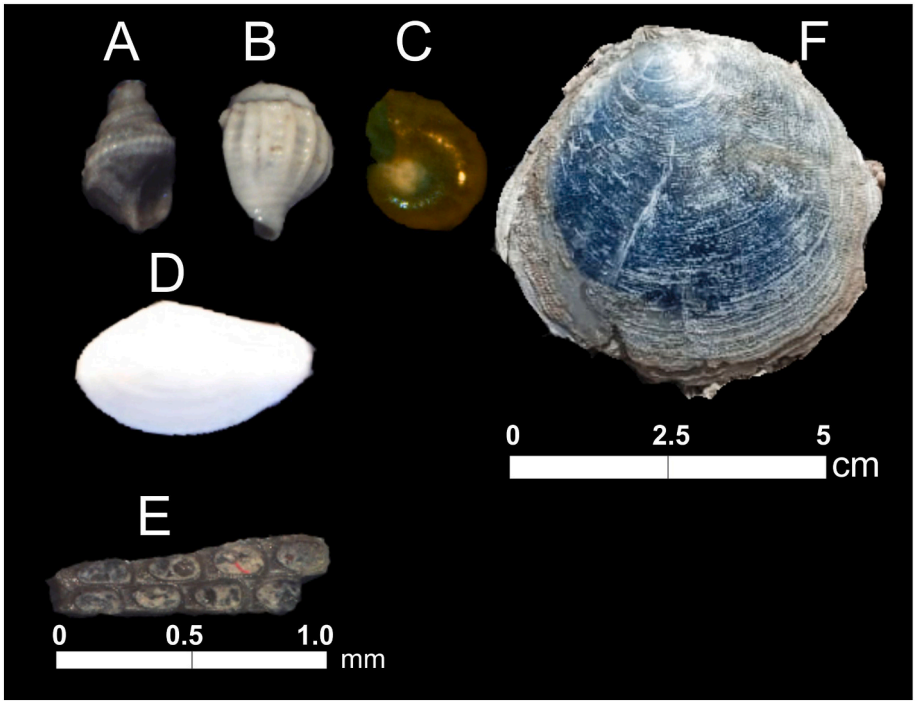

Fig. 4. Important marine fauna recorded in the Hammar Formation, A. *Nucella* sp., B. *Alvania* sp., C. *Gyaulus* sp., D. *Placuna placenta*, E. *Theora* sp., F. Bryozoa piece. A, C, and F were collected from a depth of 4 m at site #HA8, and B-E were collected from a depth of 5 m at site #HA7. Note different scale bars for A-E (0.5 mm) and F (5 cm).

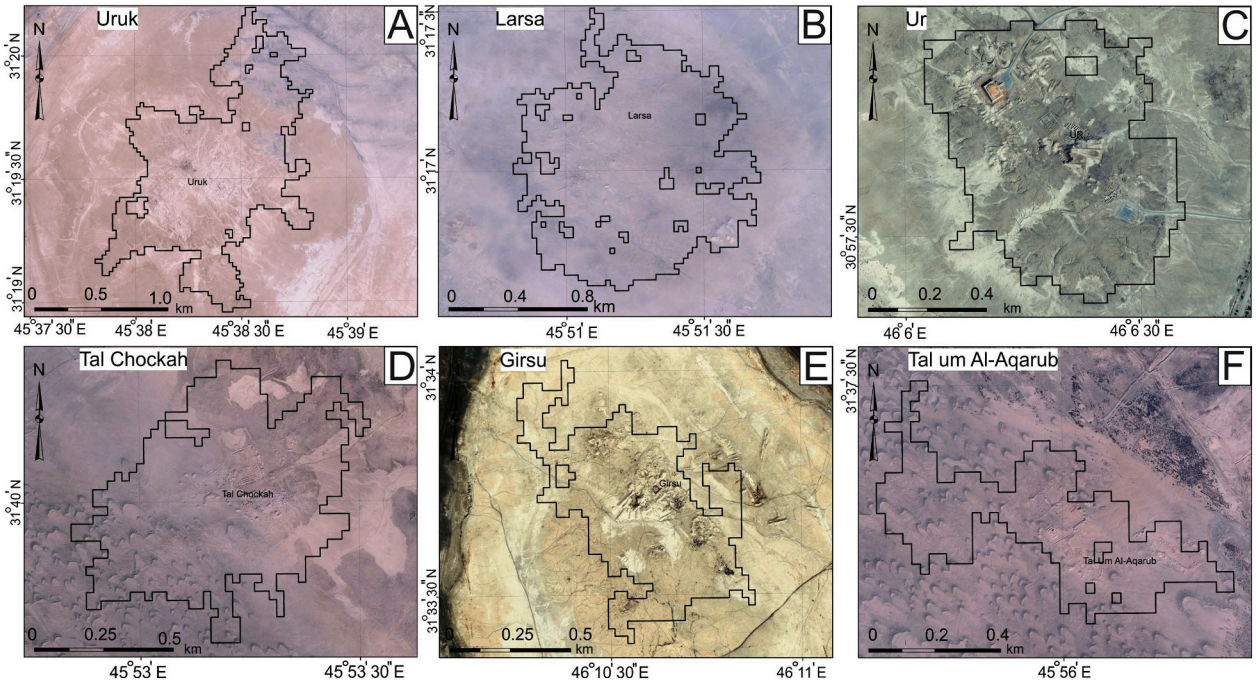

Fig. 5. QuickBird satellite image overlaid by thresholded TPI with ≥5 m elevations for the major archaeological sites.

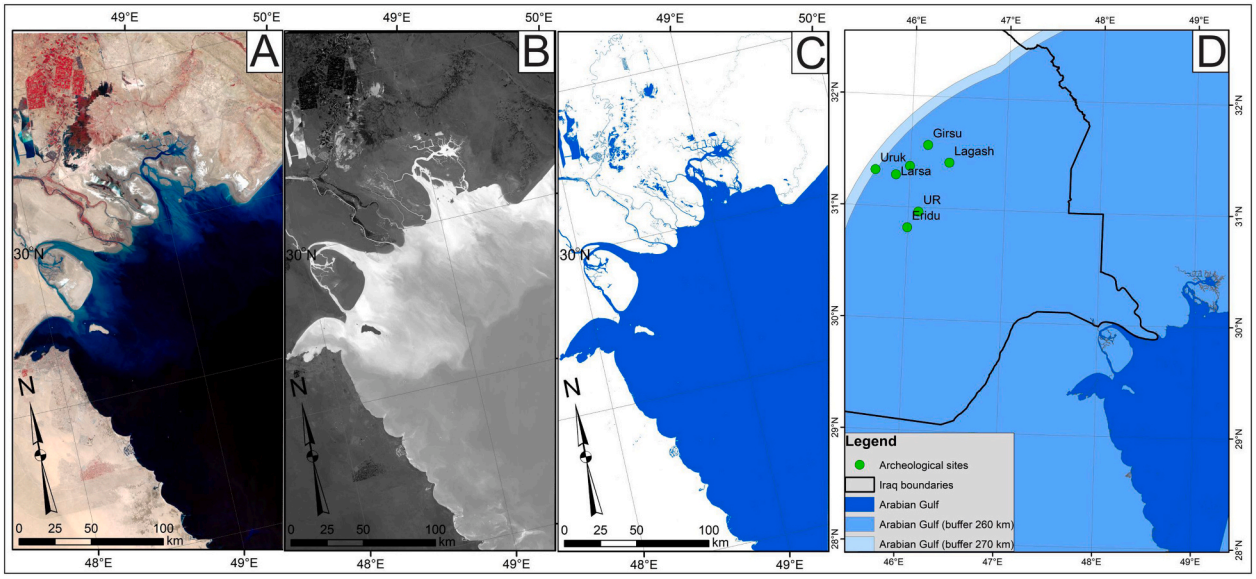

Fig. 6. (A) Landsat OLI image, (B) MNDWI, (C) vector of the MNDWI of the Gulf, and (D) the buffer of 260 km and 270 km around the Gulf.

marine waters with salinity levels ranging from 30 to 40 ‰—a range indicative of progressive marine conditions, depending on the recorded foraminifera species (Murray, 1969).

One of the most compelling indicators of marine water is the presence of planktonic foraminifera (Figs. 3J, K, and L) and Radiolaria (Figs. 3M and N), as these organisms are exclusively associated with high-salinity marine environments. Their presence serves as a critical piece of evidence, reflecting the unique ecological conditions necessary for their growth and survival in salty oceanic waters.

Elphidium excavatum (Fig. 3B) lives in the epibenthic zone on coarse sediment, especially on sandy substrates in shallow depths (< 30 m). Sometimes these species occur in intertidal to shallow subtidal water (6 m). These observations affirm that brackish estuaries and lagoons are extremely variable environments both temporally and spatially.

Al-Jumaily (1994) confirmed that the presence of various species of ostracods, including *Cyprideis torosa*, Haplocytheria keyseri, Hemicytheridea paki, Neomonoceratina iniqua, Neocytheromorpha reticulata, and Alocopocythere reticulata in conjunction with other foraminiferal species, such as *Elphidium excavatum*, *Ammonia beccarii*, and *Buccella frigida*, indicates the existence of shallow marine environments characterized by euhaline conditions, with salinity levels ranging between 30 and 40 ‰. This assemblage reflects a specific ecological setting conducive to the growth and survival of these organisms.

Additionally, the molluscan shell is indicative of marine and brackish waters, as exemplified by Placuna placenta, commonly located in shallow coastal regions with a preference for sandy or muddy substrates. This species often flourishes in estuarine environments and is capable of existing in brackish waters. It is recognized for its tolerance to varying

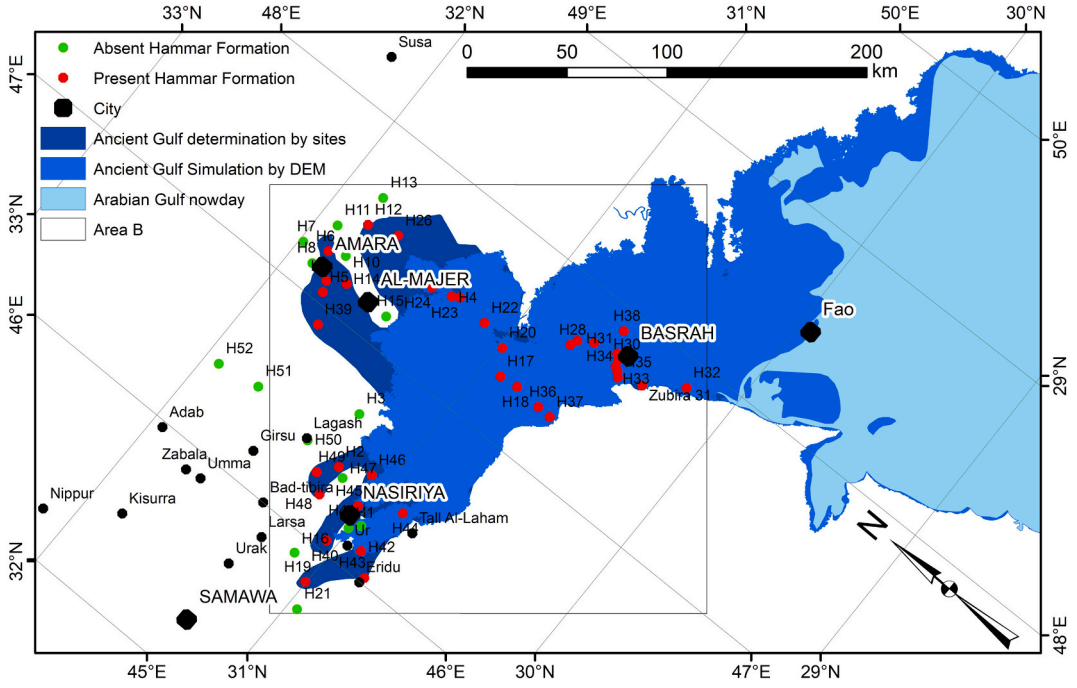

Fig. 7. Gulf paleoshoreline at 5500 ± 500 yr BP, determined by DEM and field data (Area A appears in Fig. 1).

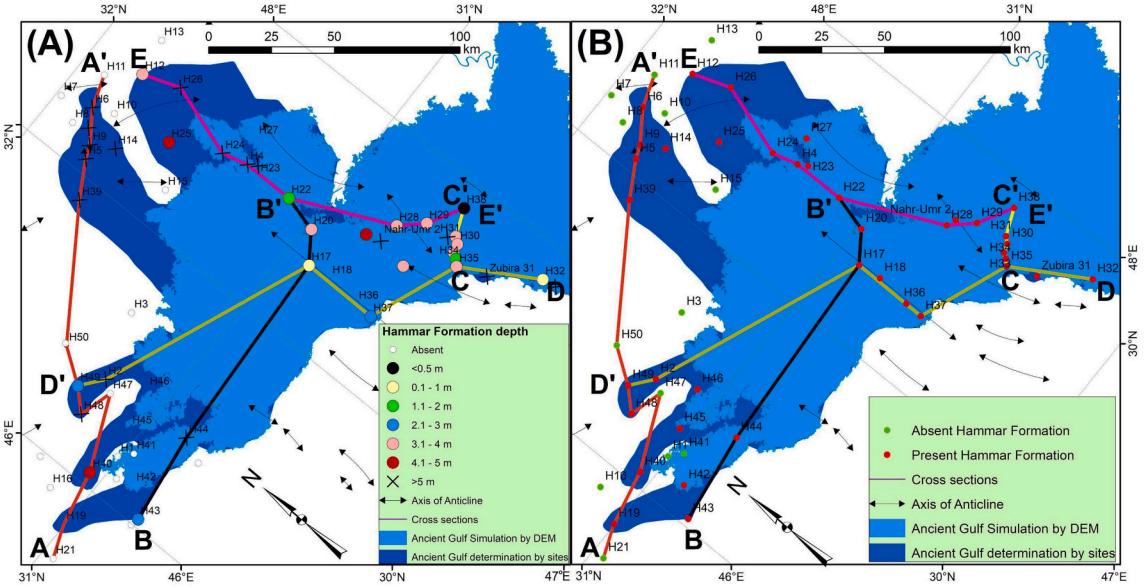

Fig. 8. (A) Cross sections and depth of the Hammar Formation determined from field data and (B) analyses of field samples (Area B appears in Figs. 1 and 6). The cross sections (A-A', B-B′, C-C′, D-D′, and E-E') of the Holocene sedimentary can be found in Fig. 12.

levels of salinity and can inhabit areas with fluctuating environmental conditions. In terms of depth, the windowpane oyster typically resides in shallow waters, usually at depths ranging from just below the intertidal zone to approximately 20 m (Mahdipour et al., 2024).

Fig. 4 shows that the distinctive organisms not only highlight the unique biodiversity of the Hammar Formation but also provide important insights into the paleoenvironmental conditions of the area.

5.2. The accuracy of ancient human settlements

The archaeological sites map with points in shapefile format did not reveal the areal extent of the Gulf at each of the studied sites. To overcome this deficiency, we used the TPI algorithm to delineate the archaeological sites. We tested the thirteen major ancient cities in Sumer, Zabala (Tal Ibzeikh), Uruk, Ur, Umma, Nippor, Marad (Tal Wannat Es-Sadum), Larsa, Lagash, Kuara (Tal Al-Lahm), Kisurra (Tal Abu Hatab), Kish, Girsu, and Adab to evaluate the TPI maps. All the TPIs' kernels detected the Ur and Uruk cities, but did not detect the Adab and Kish cities. We believe that the settlement and cultivation activities flattened the Adab and Kish cities, which rendered them virtually undetectable.

For those detected ancient cities using different kernel sizes, the number of pixels that have TPI ≥5 m increases with the kernel size. In other words, the larger the kernel size, the more pixels cover ancient cities. TPI with kernel size 201 by 201 pixels was found to be the best kernel for detecting major archaeological sites (Table 2): TPI with kernel

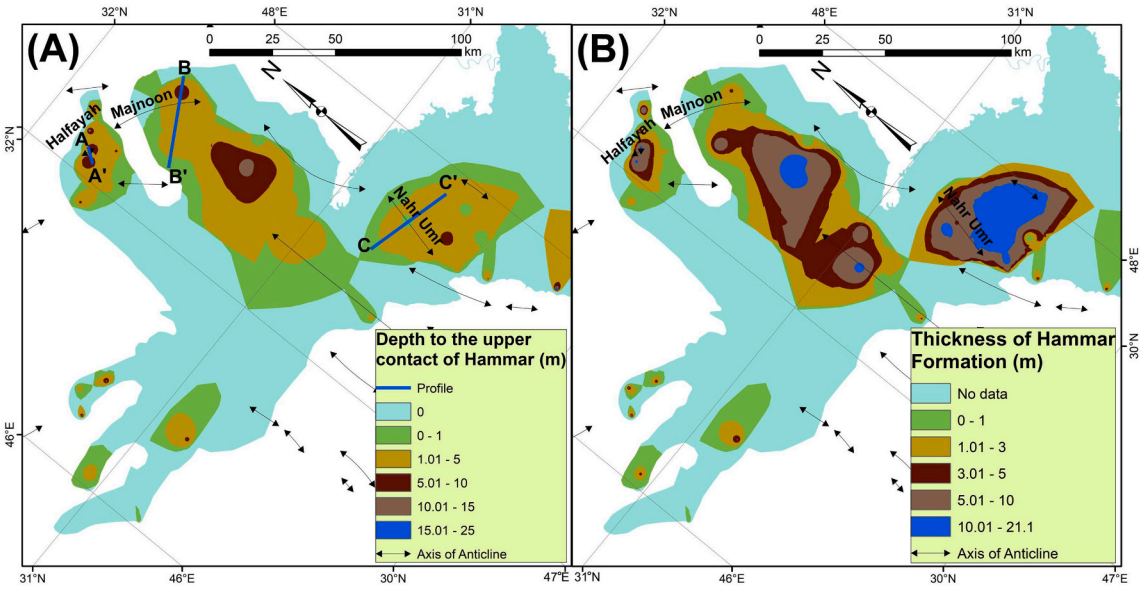

Fig. 9. IDW of (A) the depth and (B) the thickness of the Hammar Formation determined from previous data and analyses of field observations and samples collected during the fieldwork (Area B appears in Figs. 1 and 4). Subfigure A includes the location of the cross sections (A-A', B-B', and C-C') show the neotectonics activities in the Hammar Formation. These cross sections can be found in Fig. 13. The axes of the anticlines are after Fouad (2015).

Table 2
The omission accuracies of the kernel sizes used to create the TPI.

Kernel size	City present	City absent	Omission accuracy%
11	2	11	15.4
21	5	8	38.5
31	8	5	61.5
51	10	3	76.9
101	10	3	76.9
201	11	2	84.6

size 201 by 201 pixels covers almost all the areas of the cities that have been detected. The omission accuracy of the kernel size 201 by 201 pixels was 84.6 % for delineating major archaeological sites. It was difficult to estimate the commission accuracy since this kind of accuracy requires an accurate database for all archaeological sites, geomorphic features, and recent settlements. The archaeological sites detection could be improved by calculating the ratio between the length and the width of each site segment or by including additional data to remove the committed features, such as the presence of aeolian sand dunes and recent settlements. The anomalous reliefs (TPI $\geq$5 m) could be an indicator of the occurrence of archaeological sites, specifically those features with circular outlines. Thus, the TPI is useful for detecting local archaeological sites that have TPI $\geq$5 m with semi-circular and circular outlines (Fig. 5).

5.3. The Gulf paleoshoreline

According to Lambeck (1996), since the last glacial maximum, sea level has fluctuated between +5 m and − 125 m relative to the present level. He suggested that sea level rise commenced ~18,000 yr BP and advanced rapidly to near-present levels before 5500 ± 500 yr BP. At ~18,000 yr BP, the Gulf coastline was ~1000 km far south-eastward, at the Strait of Hormuz, with an average lateral advance rate of the sea levels of 125 m per year. We support the recommendation of Lambeck (1996) for further studies to reconstruct the geomorphology of the Gulf and the LMP for the precise location of ancient cities in the region.

The global wet climate for the period between 5000 and 6000 yr BP (Al-Ameri and Briant, 2019) has been recorded from several regions, e.g., Australia (Oon, 2018) and China (Yafeng et al., 1993). The transgression of the Gulf, which had reached its peak (during 5000–6000 yr BP) indicates one of the past global climate changes (Hritz et al., 2012; Al-Ameri and Briant, 2019). The Epic of Gilgamesh recorded the Mesopotamian river floods (Sumerian flood), which were put into writing nearly 3700 yr BP, including an event older than the epic (Macfadyen and Vita-Finzi, 1978). This flood happened during 4500–5500 yr BP in Ur and Kish (Ellison, 1978; Al-Ameri and Briant, 2019). We agree with Lambeck (1996), who attempted to link the Sumerian flood with the peak of the Gulf transgression as both occurred at the same time.

This study disagrees with Sarnthein (1972), Aqrawi (1995), Aqrawi (2001), Kennett and Kennett (2006), and Milli and Forti (2019) on the location of the paleoshoreline of the Gulf at 5500 ± 500 yr BP, when they stated that the paleoshoreline extended laterally between 260 and 270 km north of the present shoreline. As shown in Fig. 6D, had the paleoshoreline of the Gulf been as far away as suggested, the ancient cities of Ur, Uruk, Lagash, Girsu, Bad-Tibira, Larsa, Eridu, and Susa, would have been underwater. However, the presence of the Hammar Formation (marine sediments deposited 5500 ± 500 yr BP), as shown in this study, has provided accurate results in delineating the paleoshoreline.

Fig. 10 shows the spatial distribution of Gulf paleoshorelines at 5500 ± 500 yr BP, delineated by Sanlaville (1989), Pournelle (2003), Ur (2014), and this study. Sanlaville (1989) and Ur (2014) extend the paleoshoreline farther to the east than in this study (Fig. 10). However, the suggested paleoshoreline by Sanlaville (1989) and Ur (2014) has an elevation of 92 m and ~ 15 m asl on the east and west sides, respectively. This spatial distribution reflects the asymmetry of the paleoshoreline at sea level, which is impossible because water has the property of elevation symmetry.

The Gulf paleoshoreline outlined by Pournelle (2003) closely agrees with this study. However, Pournelle (2003) extended the paleoshoreline to the northwest, making it cover Samawa City (Fig. 10). This area is at an elevation of 11 m asl, and according to the Pournelle's (2003) suggestion, archaeological cities, including Ur, Girsu, and Lagash, would have been underwater. Our study shows that the Hammar Formation is absent from sites #H41, #H1, #H16, and #H50, which means that the paleoshoreline of the Gulf did not reach Samawa City at all. Furthermore, the information obtained from sites #H10 and #H15, as well as the results of our field studies and laboratory analyses, indicated the

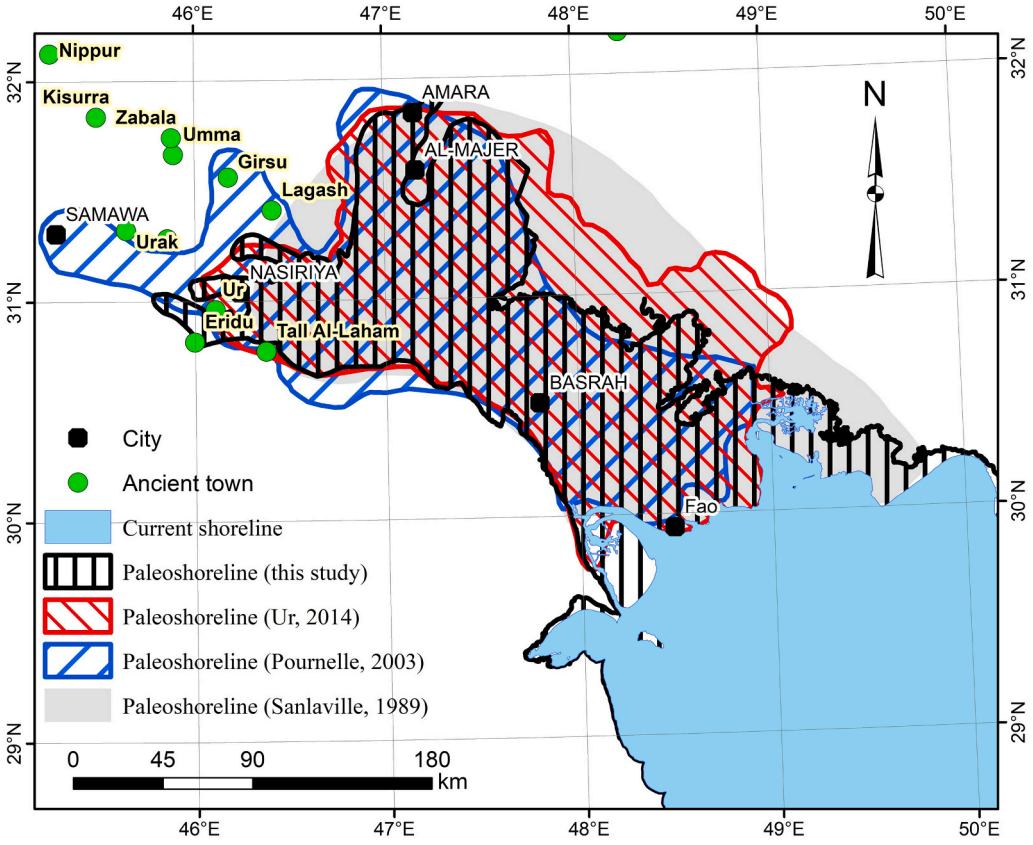

Fig. 10. Comparison between the spatial distribution of Gulf paleoshorelines during 5500 ± 500 yr BP delineated by Sanlaville (1989), Pournelle (2003), Ur (2014), and this study (2025).

presence of a tongue of land mass located in the north of the study area (close to Amara City), an occurrence that was not documented in any of the previous studies.

Our investigation revealed a mismatch between the paleoshoreline of the Gulf delineated by DEM simulation and analyses of the Hammar Formation samples collected from various sites. This mismatch was noted at two locations: In the northwest, it was induced by anthropogenic activities and deposition of aeolian sand dunes (Fig. 11), which caused an increase in the elevation of these built-up areas. This increase in elevation led to an error in the delineation of the paleoshoreline due to the altered topography of the area (Figs. 7 and 8).

The second mismatch was noted in the northern part of the study area (Figs. 7 and 8), which was caused by the uplift in the 2000 km long NW-SE trending Zagros Mountains Belt (Alavi, 2004; Othman and Gloaguen, 2013a, 2013b). The Zagros Mountains Belt and its foreland basin are the result of the ongoing collision between the Arabian and Eurasian plates at a rate of ~2–3 cm yr^{-1} (Vernant et al., 2004). For the past 55 Ma, this collision has been synchronous with progressive uplift,

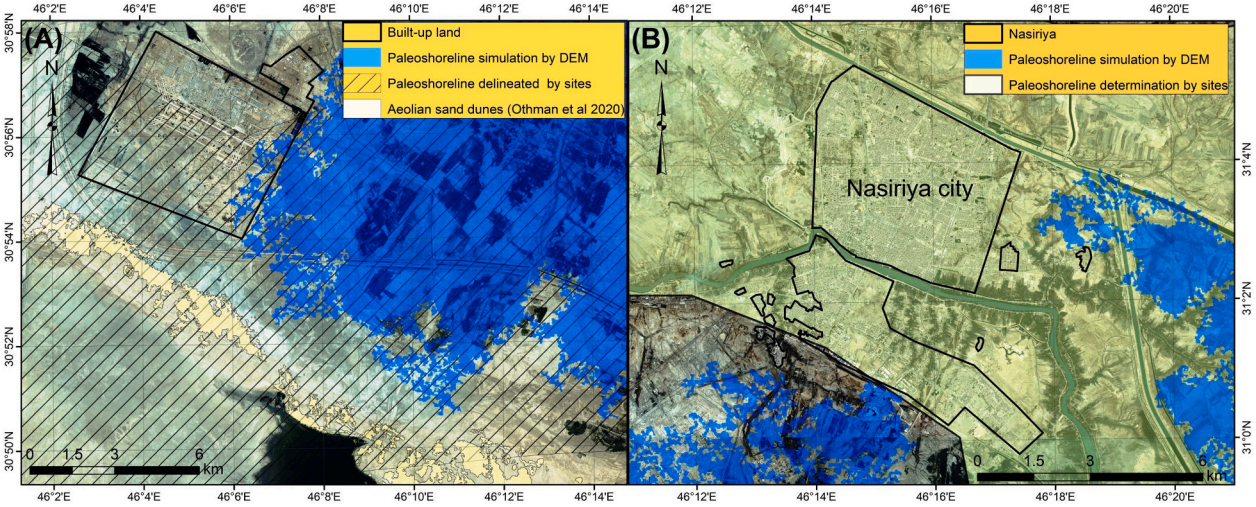

Fig. 11. QuickBird images overlayed by Gulf paleoshoreline models determined by DEM and site data for the period 5500 ± 500 yr BP. (A) shows the effects of aeolian sand dunes (from Othman et al., 2020) and anthropogenic activities; (B) shows the effect of activities by Nasiriya City. Both A and B reveal the mismatch between the two models.

manifested in both surface and subsurface structures (Mouthereau et al., 2012). One of the formations affected by this collision is the Hammar Formation. Our study confirms the presence of neotectonic deformations in the Hammar Formation, including thickening and folding of beds, which are noticeable in the Halfayah and Majnoon anticlines (Figs. 9 and 13).

5.4. Neotectonic activity

Drawing upon the information of the Tell Zurghul archaeological site (belonging to the ancient State of Lagash), Iacobucci et al. (2023) estimated that the Gulf sea level was 6 m above the present level 5500 ± 500 yr BP. We believe that the sea level value of 6 m for the Gulf at 5500 ± 500 yr BP is exaggerated because a 6 m rise of the sea level would cause most of the archaeological cities to drown in the paleo Gulf, which is not the case. Moreover, Lambeck (1996) stated that the elevation of the sea level to the north of the Gulf at 5500 ± 500 yr BP was ~3.5 m above the present level, but we hold the opinion that it was slightly lower. After the SRTM DEM simulation (LP DAAC, 2015), we concluded that 3.75 m asl was the best paleoshoreline elevation and was consistent with the paleoshoreline delineated by the Hammar Formation samples of Hudson et al. (1957), Macfadyen and Vita-Finzi (1978), Raji (1983), Yacoub et al. (1985), Yacoub (1992), Salman (1993), Aqrawi (1993), Al-Jumaily (1994), Karim et al. (1994), Aqrawi (1995), and Yacoub

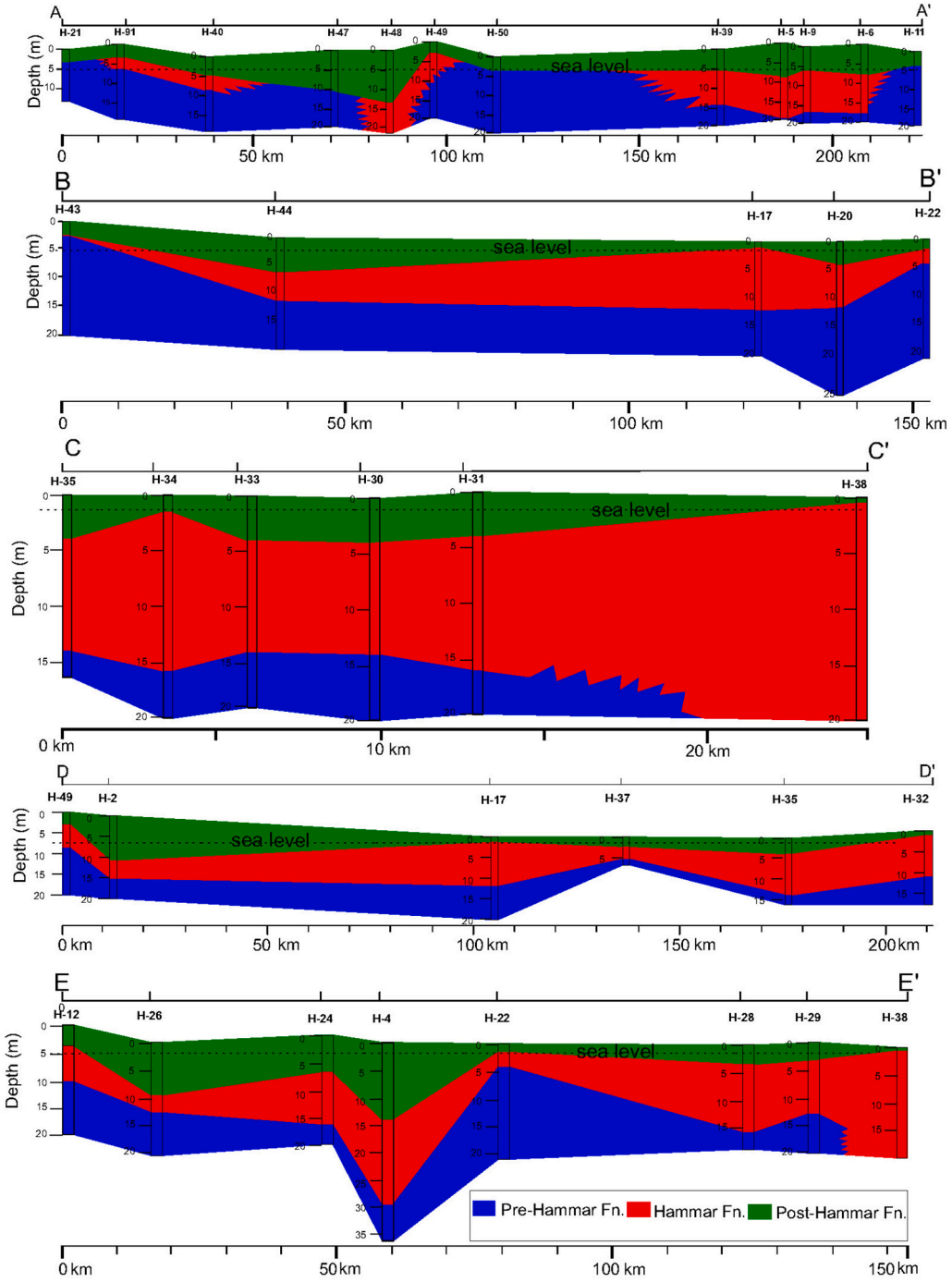

Fig. 12. Cross sections of the Holocene sedimentary units in Lower Mesopotamia. Deposition of the Hammar Formation resulted from transgression of the Gulf (the location of the cross sections can be found in Fig. 8).

(2011a).

To our knowledge, the only available dating research about the Hammar Formation is Aqrawi (1995). Two organic-rich borehole samples have been collected from the lower and upper contact of the Hammar Formation. According to the ^{14}C radiocarbon dating, the ages of the lower and upper samples were 8350 ± 230 yr BP and 5460 ± 175 yr BP, respectively (Aqrawi, 1995). However, the precise determination of the age for the Hammar Formation needs further dating (Aqrawi, 1993). The Hammar Formation took more than 2890 years to be deposited (Aqrawi, 1995). By integrating the results of Aqrawi (1995) with other published results, such as Yacoub et al. (1985), Kennett and Kennett (2006), and Milli and Forti (2019), the upper contact of the Hammar Formation was most likely to be deposited at 5500 ± 500 yr BP, hence, all deformational structures (folding) are the result of neotectonics. In this study, the determined folding corresponds with the axes of the Halfayah, Majnoon, and Nahr Umar anticlines as reported by Fouad (2015).

Fig. 12 shows sections across the Halfayah, Majnoon, and Nahr Umar anticlines, where the Hammar Formation is affected by tectonic deformation. The first two anticlines are located between Al-Amara and Al-Majer cities, while the third one is close to Basrah City.

Estimates of Holocene uplift rates have been conducted in several areas: Qatar has experienced uplift between 0.3 mm·yr^{-1} and 1.1 mm·yr^{-1} (Vita-Finzi, 1979), and Kish Island in Iran had an uplift rate between 0.13 mm·yr^{-1} and 0.24 mm·yr^{-1} (Preusser et al., 2003). Both areas are located in the southeastern part of the Zagros Range, in whose northwestern part (Safin and Sarta anticlines), the Late Pleistocene to Holocene uplift rate 0.7 ± 0.07 mm·yr^{-1} and 1.35 ± 0.2 mm·yr^{-1} (Zebari et al., 2021).

Our study is consistent with previous estimates of the uplift rate (Vita-Finzi, 1979; Preusser et al., 2003; Zebari et al., 2021) that we determined to range between ~0.33 ± 0.03 mm·yr^{-1} and 1.67 ± 0.01 mm·yr^{-1} as illustrated in Fig. 13. Cross sections (A-A'), (B-B′), and (C-C′) across the Halfayah, Majnoon, and Nahr Umar anticlines show the difference between the highest and lowest points to be 1.8 m, 9.18 m, and 3.2 m, corresponding to an uplift rate of ~0.33 ± 0.03, 1.67 ± 0.01, and 0.57 ± 0.06 mm·yr^{-1} for the Halfayah, Majnoon, and Nahr Umar anticlines, respectively (Figs. 8 and 13).

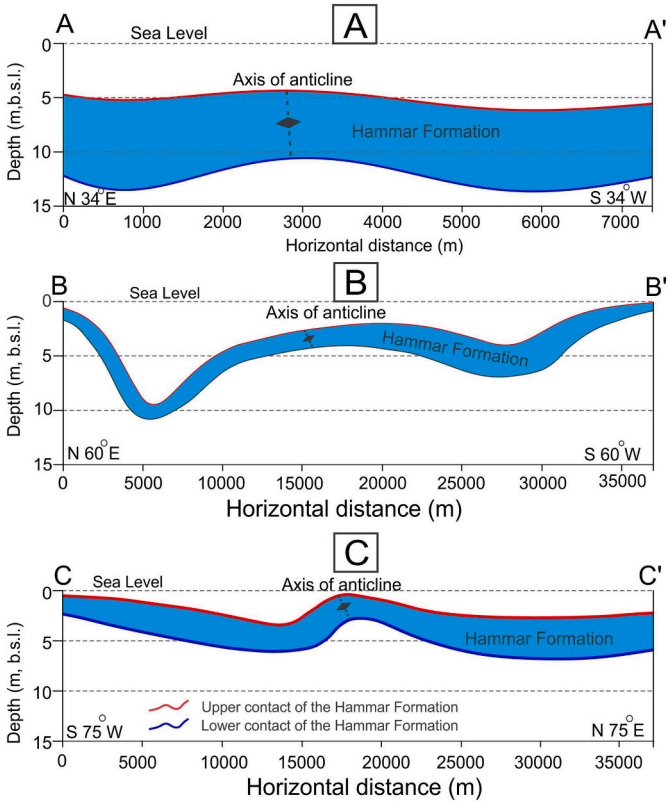

Fig. 13. Neotectonic activities in the Hammar Formation illustrated in cross sections (Axis of anticline; A B C) across the Halfayah, Majnoon, and Nahr Umar anticlines (the location of the cross sections can be found in Fig. 9A).

6. Conclusions and recommendations

Gulf shoreline transgression led to the deposition of the Hammar Formation at 5500 ± 500 yr BP. The spatial distribution of the paleoshoreline of the Gulf was determined by using two models. The first model represents a novel approach accomplished by simulating the elevation obtained from the SRTM DEM. The second model was interpolated in relation to the presence or absence of the Hammar Formation using data from previous studies and information generated from our field investigations, as well as laboratory analyses of samples collected in the field. The mismatch between the first and second models reflects the combined influence of anthropogenic activities, deposition of aeolian materials, and the uplift of the Zagros Mountains. Our results show that the Gulf paleoshoreline rose 3.75 m above its present level and was located about 190 and 230 km (not 260-270 km) northwest of the present-day shoreline that covered the Lower Mesopotamian Plain. Our findings on the accurate delineation of the Gulf paleoshoreline are of great significance as they will enable the enhancement of archaeological and historical information relating to the major Sumerian cities, such as Eridu, Lagash, Larsa, Ur, and Uruk, which were built along and close to the Gulf shoreline.

The Topographic Position Index (TPI) has been used to establish the locations of major archaeological sites at ~5 m higher than the surrounding area. The TPI with kernel size 201 by 201 was useful in delineating almost all archaeological sites with an omission accuracy of 84.6 %. The TPI kernel size has a direct relationship to the elevation of anthropogenic sites. Due to the incomplete information on recent anthropic activities and aeolian sand dunes in the archaeological site's database, it was not easy to estimate the accuracy of TPI results. We recommend further studies to determine the precise rate of uplift in the Lower Mesopotamian region. In addition, the accurate location of anthropogenic sites could be improved by a more precise determination of the areal extent of archaeological sites using additional data to remove unwanted features, such as sand dunes and human settlements. Nonetheless, our study demonstrates that integrating digital remote sensing, GIS, and archaeological information will be valuable for gaining a clear understanding of the lives and cultures of people who inhabited one of the most prominent regions in human civilizations.

Folding observed in the Hammar Formation confirms that the study area underwent neotectonic activity, especially in the eastern parts. The uplift rates of the Halfayah, Majnoon, and Nahr Umar anticlines are ~0.33 ± 0.03 mm·yr^{-1}, 1.67 ± 0.01 mm·yr^{-1}, and 0.57 ± 0.06 mm·yr^{-1}, respectively.

CRediT authorship contribution statement

Arsalan Ahmed Othman: Visualization, Validation, Supervision, Software, Resources, Project administration, Methodology, Investigation, Funding acquisition, Formal analysis, Data curation, Conceptualization, Writing – review & editing, Writing – original draft. **Salahalddin S. Ali:** Resources, Methodology, Funding acquisition, Writing – review & editing, Writing – original draft. **Ahmed K. Obaid:** Software, Investigation, Writing – review & editing. **Younus I. Al-Saady:** Software, Investigation, Conceptualization, Writing – review & editing. **Maher M. Mahdi:** Methodology, Investigation, Writing – review & editing. **Mustafa Ali:** Resources, Investigation, Writing – review & editing. **Hasan Kattoof Jasim:** Investigation, Formal analysis, Writing – review & editing. **Syed E. Hasan:** Investigation, Writing – review & editing. **Veraldo Liesenberg:** Software, Writing – review & editing.

Declaration of competing interest

No potential conflict of interest was reported by the author(s).

Acknowledgments

The authors would like to thank the two anonymous reviewers for their insightful comments that have greatly enhanced the quality of this article. We also thank the United States Geological Survey for Landsat and DEM data and the European Space Agency for the Sentinel-2A data.

Appendix

Appendix 1

Foraminifera and Ostracoda species in the previous (Al-Jumaily, 1994; Al-Jaberi and Mahdi, 2020) and current study.

Foraminifera species (Al-Jaberi and Mahdi, 2020; Fig. 2)	Ostracoda species (Al-Jumaily, 1994; Fig. 2)	Foraminifera and Ostracoda species (current study)
		Foraminifera species
Ammonia beccarii	*Alocopocythere reticulata*	*Ammonia beccarii* Fig. 2A
A.tepida	*Candona neglecta*	*A.Parkinsoniana* Fig. 2B
A.parkinsoniana	*Candona sp*	*Ammonia tepida* Fig. 2C and 3H
A.hozanensis	*Candoniella simpsoni*	*Buccella frigida* Fig. 3D
A.nipponica	*Carinocythereis indica*	*Elphidium advenum* Fig. 2D
Asterorotalia sp	*Chrysocythere keiji,*	*Elphidium lessonii* Fig. 2F
Buccella frigida	*Cyprideis torosa*	*Elphidium incertum* Fig. 2F
Elphidium incertum	*C. torosa var torosa*	*Elphidium excavatum* (Fig. 3B
E.gunteri	*Cyprintous scholiosa*	*Haynesina* sp. Fig. 3 A and G
E.poeyanum	*Cyprintous salinus*	*Quinqueloculina poeyana* Fig. 2G
E.advanum	*Cushmanidae guhai*	*Quinqueloculina poeyana* (Fig. 2G
E.lesson	*Drawinula stevensoni*	*Rosalina williansoni* (Fig. 3E
E.excavatum	*Haplocythereidae keyser*	*Spiroloculina Laevigata* Fig. 2H & 2O
Bolivina sp	*Hemicytheridea paiki*	*Triloculina oblonga* Fig. 3Q
Discorps todda	*Hemikirthe peterseni*	Planktonic genera Fig. 3J, K, and L
Lagena sp	*Hemicytheridea reticulata*	Ostracoda species
Miliammina fusca	*Kerthe sp*	*Alocopocythere reticulate* Fig. 3R
Nonionella caspia	*Leguminocythereis papuensis*	*Carinocythereis indica Fig. L*
Quinqueloculina seminula	*Limnocythere inopenata*	*Cyprideis torosa (*Figs. 2I and *3*S
Q.elongate	*Illyocypris monstrifica*	*Haplocytheria keyseri* Fig. *3 T*
Q.laevigata	*Illyocypris gibba,*	*Hemicytheridea paki* Fig. 2 K
Q.lamarkiana	*Illyocypris bradyi,*	*Loxoconcha* sp. Fig. 2 R
Q.buchiana	*Loxochoncha* sp.,	*Mediocytherideis seminist* Fig. 2 *N.*
Q.stalkeri	*Neomonceratina iniqua*	*Neomonoceratina iniqua* Fig. 2 M
Q.ovula	*Tyrrhenocythere amnicola*	*Neocytheromorpha reticulata* Fig. 2 O
Pyrgo sp		*Neomonoceratina delicate* Fig. 2 Q
Triloculina oblonga		
T.rotunda		
Spiroloculina laevigata		
S.exima		

Data availability

Data will be made available on request.

References

Agapiou, A., Lysandrou, V., 2020. Detecting Displacements within Archaeological Sites in Cyprus after a 5.6 Magnitude Scale Earthquake event through the Hybrid Pluggable Processing Pipeline (HyP3) Cloud-based System and Sentinel-1 Interferometric Synthetic Aperture Radar (InSAR) analysis. IEEE J. Sel. Top. Appl. Earth Obs. Remote Sens. 13, 6115–6123. https://doi.org/10.1109/JSTARS.2020.3028272.

Al-Ameri, I.D.S., Briant, R.M., 2019. A late Holocene molluscan-based palaeoenvironmental reconstruction from southern Mesopotamia: Implications for the palaeogeographic evolution of the Arabo-Persian Gulf. J. African Earth Sci. 152, 1–9. https://doi.org/10.1016/j.jafrearsci.2018.12.012.

Alavi, M., 1994. Tectonics of the Zagros Orogenic Belt of Iran: New data and interpretations. Tectonophysics 229, 211–238. https://doi.org/10.1016/0040-1951(94)90030-2.

Alavi, M., 2004. Regional stratigraphy of the Zagros fold-thrust belt of Iran and its proforeland evolution. Am. J. Sci. 304, 1–20. https://doi.org/10.2475/ajs.304.1.1.

Alavi, M., 2007. Structures of the Zagros Fold-Thrust Belt in Iran. Am. J. Sci. 307, 1064–1095. https://doi.org/10.2475/09.2007.02.

Al-Jaberi, M.H., Mahdi, M.M., 2020. Mineralogy and paleontology of the Quaternary sediments in Karmat Ali at Basrah. Southern Iraq. Iraqi Geol. J. 105–120.

Al-Jumaily, W.A., 1994. Quaternary Ostracods in Southern Iraq. University of Baghdad, Unpub.

Al-Shawi, Z.A.A., Mahdi, M.M., Mohammed, A.H., 2019. New records of planktonic foraminifera in the Shuaiba Formation (Aptian Age), Mesopotamian plain. South of Iraq. Iraqi J. Sci. 1322–1335.

Aqrawi, A.A.M., 1993. Recent Sediments of the Tigris-Euphrates Delta: The Southern Marshlands (Ahwar). University of London.

Aqrawi, A.A.M., 1995. Correction of Holocene sedimentation rates for mechanical compaction: the Tigris-Euphrates Delta, lower Mesopotamia. Mar. Pet. Geol. 12, 409–416. https://doi.org/10.1016/0264-8172(95)96903-4.

Aqrawi, A.A.M., 2001. Stratigraphic signatures of climatic change during the Holocene evolution of the Tigris–Euphrates delta, lower Mesopotamia. Glob. Planet. Chang. 28, 267–283. https://doi.org/10.1016/S0921-8181(00)00078-3.

Beke, C.T., 1835. VI. On the geological evidence of the advance of the land at the head of the Persian Gulf. London, Edinburgh. Dublin Philos. Mag. J. Sci. 7, 40–46. https://doi.org/10.1080/14786443508648653.

Ben-Romdhane, H., Francis, D., Cherif, C., Pavlopoulos, K., Ghedira, H., Griffiths, S., 2023. Detecting and Predicting Archaeological Sites Using Remote Sensing and Machine Learning—Application to the Saruq Al-Hadid Site. Geosciences, Dubai, UAE. https://doi.org/10.3390/geosciences13060179.

Berberian, M., 1995. Master "blind" thrust faults hidden under the Zagros folds: active basement tectonics and surface morphotectonics. Tectonophysics 241. https://doi.org/10.1016/0040-1951(94)00185-C.

Cooke, G.A., 1987. Reconstruction of the Holocene coastline of Mesopotamia. Geoarchaeology 2, 15–28. https://doi.org/10.1002/gea.3340020102.
Directorate of Antiquities, 1976. Iraq Atlas Archaeological Sites (Baghdad-Iraq).
Ellison, E.R., 1978. A study of diet in Mesopotamia (c.3000-600 BC) and associated agricultural techniques and methods of food preparation of food preparation.
ESRI, 2021. ArcGIS Desktop. Release 10.8.2.
Exelis Visual Information Solutions, 2015. ENVI V. 5.2, NV5 Geospatial Software, Boulder, Colorado.
Felde, G.W., Anderson, G.P., Cooley, T.W., Matthew, M.W., adler-Golden, S.M., Berk, A., Lee, J., 2003. Analysis of Hyperion data with the FLAASH atmospheric correction algorithm, in: Geoscience and Remote Sensing Symposium, 2003. IGARSS '03. Proceedings. 2003 IEEE International. pp. 90–92 vol.1. https://doi.org/10.1109/IGARSS.2003.1293688.
Forti, L., Romano, L., Celant, A., D'Agostino, F., Di Rita, F., Jotheri, J., Magri, D., Mazzini, I., Tentori, D., Milli, S., 2022. The paleoenvironment and depositional context of the Sumerian site of Abu Tbeirah (Nasiriyah, southern Mesopotamia, Iraq). Quat. Res. 110, 165–183. https://doi.org/10.1017/qua.2022.22.
Fouad, S.F., Sissakian, V.K., 2011. Tectonic and structural evolution of the Mesopotamia Plain. Iraqi Bull. Geol. Mining. Spec. issue 4, 33–46.
Fouad, S.F.A., 2015. Tectonic map of Iraq, scale 1: 1000 000, 2012. Iraqi Bull. Geol. Min. 11, 1–7.
Green, O.R., 2013. A Manual of Practical Laboratory and Field Techniques in Palaeobiology. Springer Science & Business Media.
Heyvaert, V.M.A., Baeteman, C., 2007. Holocene sedimentary evolution and palaeocoastlines of the lower Khuzestan plain (Southwest Iran). Mar. Geol. 242, 83–108. https://doi.org/10.1016/j.margeo.2007.01.008.
Hritz, C., Pournelle, J., Smith, J., Albadran, B., Issa, B.M., Al-Handal, A., 2012. Mid-Holocene Dates for Organic-Rich Sediment, Palustrine Shell, and Charcoal from Southern Iraq. Radiocarbon 54, 65–79. https://doi.org/10.2458/azu_js_rc.v54i1.12362.
Hudson, R.G.S., Eames, F.E., Wilkins, G.L., 1957. The Fauna of some recent Marine Deposits near Basrah. Iraq. Geol. Mag. 94, 393–401. https://doi.org/10.1017/S0016756800069429.
Iacobucci, G., Troiani, F., Milli, S., Nadali, D., 2023. Geomorphology of the lower Mesopotamian plain at tell Zurghul archaeological site. J. Maps 19, 2112772. https://doi.org/10.1080/17445647.2022.2112772.
Jacobsen, T., 1960. The waters of Ur. Iraq 22, 174–185.
Jotheri, J., Altaweel, M., Tuji, A., Anma, R., Pennington, B., Rost, S., Watanabe, C., 2018. Holocene fluvial and anthropogenic processes in the region of Uruk in southern Mesopotamia. Quat. Int. 483, 57–69. https://doi.org/10.1016/j.quaint.2017.11.037.
Kadhim, I., Abed, F.M., 2023. A critical Review of Remote Sensing Approaches and Deep Learning Techniques in Archaeology. Sensors. https://doi.org/10.3390/s23062918.
Karim, S.A., Al-Jumaily, W.A., Al-Sheikhly, S.S., 1994. Quaternary foraminifera of Basrah area. Iraqi Geol. J. 27, 1–13.
Karymbalis, E., Papanastassiou, D., Gaki-Papanastassiou, K., Tsanakas, K., Maroukian, H., 2013. Geomorphological study of Cephalonia Island, Ionian Sea. Western Greece. J. Maps 9, 121–134. https://doi.org/10.1080/17445647.2012.758423.
Keller, E.A., Pinter, N., 2002. Active Tectonics Earthquakes, Uplift, and Landscape. In: Environmental & Engineering Geoscience, Second. ed. Printice Hall, New Jersy. https://doi.org/10.2113/gseegeosci.iii.3.463.
Kennett, D.J., Kennett, J.P., 2006. Early State Formation in Southern Mesopotamia: Sea Levels, Shorelines, and climate Change. J. Island Coast. Archaeol. 1, 67–99. https://doi.org/10.1080/15564890600586283.
Łabuz, A., Borowiec, N., Marmol, U., 2023. Automatic detection of Lusatian culture fortified settlement based on data from airborne laser scanning. Int. J. Conserv. Sci. 14, 83–98. https://doi.org/10.36868/IJCS.2023.01.07.
Lambeck, K., 1996. Shoreline reconstructions for the Persian Gulf since the last glacial maximum. Earth Planet. Sci. Lett. 142, 43–57. https://doi.org/10.1016/0012-821X(96)00069-6.
Larsen, C.E., 1975. The Mesopotamian delta region: a reconsideration of Lees and Falcon. J. Am. Orient. Soc. 43–57.
Levin, H.L., King Jr., D.T., 2016. The Earth through Time. John Wiley & Sons.
LP DAAC, 2015. The shuttle Radar Topography Mission (SRTM) Collection User Guide [WWW Document]. https://lpdaac.usgs.gov/documents/179/SRTM_User_Guide_V3.pdf.
Macfadyen, W.A., Vita-Finzi, C., 1978. Mesopotamia: the Tigris—Euphrates delta and its Holocene Hammar fauna. Geol. Mag. 115, 287–300. https://doi.org/10.1017/S0016756800037183.
Mahdipour, F., Bahrami, A., Yazdi, M., Vaziri-Moghaddam, H., Bitner, A., Vega, F., 2024. First report of the bivalve Placuna placenta (Linnaeus, 1758) from the Late Miocene–Early Pliocene strata of the Minab region and Qeshm Island, Persian Gulf, Southern Iran: Palaeoecology, systematic and taphonomy. J. Stratigr. Sedimentol. Res. 40, 41–62.
McQuarrie, N., 2004. Crustal scale geometry of the Zagros fold-thrust belt. Iran. J. Struct. Geol. 26, 519–535. https://doi.org/10.1016/j.jsg.2003.08.009.
Milli, S., Forti, L., 2019. Geology and Palaeoenvironment of Nasiriyah Area/Southern Mesopotamia, in: D'Agostino, L.R. and F., University (Eds.), Abu Tbeirah Excavations I. Area 1 Last Phase and Building A – Phase 1. Sapienza Università Editrice, Roma, p. 477.
Mouthereau, F., Lacombe, O., Vergés, J., 2012. Building the Zagros collisional orogen: timing, strain distribution and the dynamics of Arabia/Eurasia plate convergence. Tectonophysics 532–535, 27–60. https://doi.org/10.1016/j.tecto.2012.01.022.
Murray, J.W., 1969. Recent foraminifers from the Atlantic continental shelf of the United States. Micropaleontology 401–419.
Obaid, A.K., Allen, M.B., 2017. Landscape maturity, fold growth sequence and structural style in the Kirkuk Embayment of the Zagros, northern Iraq. Tectonophysics 717, 27–40. https://doi.org/10.1016/j.tecto.2017.07.006.
Obaid, A.K., Allen, M.B., 2019. Landscape Expressions of Tectonics in the Zagros Fold-and-Thrust Belt. Tectonophysics 766. https://doi.org/10.1016/j.tecto.2019.05.024.
Oon, S., 2018. Holocene Sea Level Change in Northeastern Australia: A High-Resolution Record from Albatross Bay, Cape York Peninsula. Ph. D. thesis,. Department of Environmental Sciences. Macquarie University.
Othman, A.A., Gloaguen, R., 2013a. River courses affected by landslides and implications for hazard assessment: a high resolution remote sensing case study in NE Iraq-W Iran. Remote Sens. 5, 1024–1044. https://doi.org/10.3390/rs5031024.
Othman, A.A., Gloaguen, R., 2013b. Automatic Extraction and Size Distribution of Landslides in Kurdistan Region. Remote Sens, NE Iraq. https://doi.org/10.3390/rs5052389.
Othman, A.A., Gloaguen, R., 2014. Improving lithological mapping by SVM classification of spectral and morphological features: the discovery of a new chromite body in the Mawat ophiolite complex (Kurdistan, NE Iraq). Remote Sens. 6, 6867–6896. https://doi.org/10.3390/rs6086867.
Othman, A.A., Gloaguen, R., 2017. Integration of Spectral, Spatial and Morphometric Data into Lithological Mapping: A Comparison of Different Machine Learning Algorithms in the Kurdistan Region. J. Asian Earth Sci, NE Iraq. https://doi.org/10.1016/j.jseaes.2017.05.005.
Othman, A.A., Gloaguen, R., Andreani, L., Rahnama, M., 2018. Improving landslide susceptibility mapping using morphometric features in the Mawat area, Kurdistan Region, NE Iraq: Comparison of different statistical models. Geomorphology 319, 147–160. https://doi.org/10.1016/j.geomorph.2018.07.018.
Othman, A.A., Al-Maamar, A.F., Al-Manmi, D.A.M., Liesenberg, V., Hasan, S., Al-Saady, Y.I., Shihab, A.T., Khwedim, K., 2019. Application of DInSAR-PSI Technology for Deformation Monitoring of the Mosul Dam. Iraq. Remote Sens. 11, 20.
Othman, A.A., Al-Saady, Y.I., Shihab, A.T., Al-Maamar, A.F., 2020. In: Al-Quraishi, A.M. F., Negm, A.M. (Eds.), The Aeolian Sand Dunes in Iraq: A New Insight BT-Environmental Remote Sensing and GIS in Iraq. Springer International Publishing, Cham, pp. 279–300. https://doi.org/10.1007/978-3-030-21344-2_12.
Othman, A.A., Ali, S.S., Obaid, A.K., Salar, S.G., Al-Kakey, O., Al-Saady, Y.I., Latif, S.D., Liesenberg, V., Neto, S.L.R., Breunig, F.M., Hasan, S.E., 2024. Satellite-Derived Shallow Water Depths Estimation using Remote Sensing and Artificial Intelligence Models, a Case Study: Darbandikhan Lake Upper, Kurdistan Region. Iraq. Remote Sens. Appl. Soc. Environ. 101432. https://doi.org/10.1016/j.rsase.2024.101432.
Othman, A.A., Sidiq, H., Ali, S.S., Obaid, A.K., Liesenberg, V., 2025. Machine Learning for Onshore Oil Seeps Detection: a Case Study in Kirkuk-Sulaimaniyah Area. Northeastern Iraq. SPE J. 1–13. https://doi.org/10.2118/226184-PA.
Parker, A.G., Morley, M.W., Armitage, S.J., Engel, M., Parton, A., Preston, G.W., Russ, H., Drechsler, P., 2020. Palaeoenvironmental and sea level changes during the Holocene in eastern Saudi Arabia and their implications for Neolithic populations. Quat. Sci. Rev. 249, 106618. https://doi.org/10.1016/j.quascirev.2020.106618.
Pour, A.B., Ranjbar, H., Sekandari, M., Abd El-Wahed, M., Hossain, M.S., Hashim, M., Yousefi, M., Zoheir, B., Wambo, J.D.T., Muslim, A.M., 2023. 2 - Remote sensing for mineral exploration, in: Pour, A.B., Parsa, M., Eldosouky, A.M.B.T.-G.A.A. to M.E. (Eds.). Elsevier, pp. 17–149. https://doi.org/10.1016/B978-0-323-95608-6.00002-0.
Pournelle, J.R., 2003. Marshland of Cities: Deltaic Landscapes and the Evolution of Early Mesopotamian Civilization. UNIVERSITY OF CALIFORNIA, SAN DIEGO.
Preusser, F., Radtke, U., Fontugne, M., Haghipour, A., Hilgers, A., Kasper, H.U., Nazari, H., Pirazzoli, P.A., 2003. ESR dating of raised coral reefs from Kish Island, Persian Gulf. Quat. Sci. Rev. 22, 1317–1322. https://doi.org/10.1016/S0277-3791(03)00038-6.
Raji, W., 1983. Paleontological and Environmental Study of the Mesopotamian Plain in Samawa-Nasiriya Area. Baghdad-Iraq.
Reyss, J.L., Pirazzoli, P.A., Haghipour, A., Hatté, C., Fontugne, M., 1999. Quaternary marine terraces and tectonic uplift rates on the south coast of Iran. Geol. Soc. London. Spec. Publ. 146, 225–237. https://doi.org/10.1144/GSL.SP.1999.146.01.13.
RockWare, 2024. Rockworks. Version 16; Golden, CO 80401, USA. https://www.rockware.com/product/rockworks/.
Rohling, E.J., Cooke, S., 2003. In: Sen Gupta, B.K. (Ed.), Stable Oxygen and Carbon Isotopes in Foraminiferal Carbonate Shells BT - Modern Foraminifera. Springer, Netherlands, Dordrecht, pp. 239–258. https://doi.org/10.1007/0-306-48104-9_14.
Salar, S.G., Othman, A.A., Rasooli, S., Ali, S.S., Al-Attar, Z.T., Liesenberg, V., 2022. GIS-Based Modeling for Vegetated Land Fire Prediction in Qaradagh Area. Sustain, Kurdistan Region, Iraq. https://doi.org/10.3390/su14106194.
Salman, B., 1993. Re-Interpretation of the Ecology of the Hammar Formation from Subsurface Section in Amarah-Basrah Area, Iraq. GESURV report #2085.. Baghdad-Iraq.
Salman, B., 1997. Palynological Evidences on the Climatic and Environmental Changes during the Quaternary Period in the Mesopotamian Plain Southern Iraq. University of Baghdad.
Sanlaville, P., 1989. Considérations sur l'évolution de la basse Mésopotamie au cours des derniers millénaires. Paléorient 5–27.
Sarnthein, M., 1972. Sediments and history of the Postglacial transgression in the Persian Gulf and Northwest Gulf of Oman. Mar. Geol. 12, 245–266. https://doi.org/10.1016/0025-3227(72)90002-3.
Shareef, N.F., Mahdi, M.M., 2015. Studying of recent environments in Faw, Khor Al-Zubair and Um-Qaser areas, Southwestern Arabian Gulf, Basrah. Iraq. J. Basrah Res. 41, 1–14.
Teller, J.T., Glennie, K.W., Lancaster, N., Singhvi, A.K., 2000. Calcareous dunes of the United Arab Emirates and Noah's Flood: the postglacial reflooding of the Persian

(Arabian) Gulf. Quat. Int. 68–71, 297–308. https://doi.org/10.1016/S1040-6182(00)00052-5.
Thompson, A.E., 2020. Detecting Classic Maya Settlements with Lidar-Derived Relief Visualizations. Remote Sens. https://doi.org/10.3390/rs12172838.
Ur, J., 2014. Households and the Emergence of Cities in Ancient Mesopotamia. Camb. Archaeol. J. 24, 249–268. https://doi.org/10.1017/S095977431400047X.
Vernant, P., Nilforoushan, F., Hatzfeld, D., Abbassi, M.R., Vigny, C., Masson, F., Nankali, H., Martinod, J., Ashtiani, A., Bayer, R., Tavakoli, F., Chéry, J., 2004. Present-Day Crustal Deformation and Plate Kinematics in the Middle East Constrained by GPS Measurements in Iran and Northern Oman. Geophys. J. Int. 157, 381–398. https://doi.org/10.1111/j.1365-246X.2004.02222.x.
Vita-Finzi, C., 1979. Rates of Holocene folding in the coastal Zagros near Bandar Abbas. Iran. Nature 278, 632–634. https://doi.org/10.1038/278632a0.
Weiss, A.D., 2001. Topographic position and landforms analysis, in: ESRI Users Conference. San Diego, CA.
Xu, H., 2006. Modification of normalised difference water index (NDWI) to enhance open water features in remotely sensed imagery. Int. J. Remote Sens. 27, 3025–3033. https://doi.org/10.1080/01431160600589179.
Yacoub, S.Y., 1992. The Geology of Al-Basrah. Abadan and Bubyian Quadrangle, Baghdad-Iraq.
Yacoub, S.Y., 2011a. Stratigraphy of the Mesopotamia plain. Iraqi Bull. Geol. Min. 4, 47–82.
Yacoub, S.Y., 2011b. Geomorphology of the Mesopotamia plain. Iraqi Bull. Geol. Min. Spec. Issue 4, 7–32.
Yacoub, S.Y., Roffa, S.H., Tawfiq, J.M., 1985. The Geology Al-Amara – Nasiriyah – Al-Basrah Area. GESURV report #1386.. Baghdad-Iraq.
Yafeng, S., Zhaozheng, K., Sumin, W., Lingyu, T., Fubao, W., Tandong, Y., Xitao, Z., Peiyuan, Z., Shaohua, S., 1993. Mid-Holocene climates and environments in China. Glob. Planet. Chang. 7, 219–233. https://doi.org/10.1016/0921-8181(93)90052-P.
Zebari, M., Preusser, F., Grützner, C., Navabpour, P., Ustaszewski, K., 2021. Late Pleistocene-Holocene Slip rates in the Northwestern Zagros Mountains (Kurdistan Region of Iraq) Derived from Luminescence Dating of River Terraces and Structural Modeling. Tectonics 40. https://doi.org/10.1029/2020TC006565.